Spectroscopic Studies of Nickel-Deficient Carbon Monoxide Dehydrogenase from *Rhodospirillum rubrum*: Nature of the Iron−Sulfur Clusters[†]

Jennifer L. Craft,[‡] Paul W. Ludden,[§] and Thomas C. Brunold*[,‡]

Departments of Chemistry and Biochemistry, University of Wisconsin, Madison, Wisconsin 53706

Received July 31, 2001

ABSTRACT: Carbon monoxide dehydrogenase (CODH) from *Rhodospirillum rubrum* utilizes three types of Fe-S clusters to catalyze the reversible oxidation of CO to CO_2: a novel [Ni4Fe5S] active site (C cluster) and two distinct [4Fe4S] electron-transfer sites (B and D clusters). While recent X-ray data show the geometric arrangement of the five metal centers at the C cluster, electronic structures of the various [Ni4Fe5S] oxidation states remain ambiguous. These studies report magnetic circular dichroism (MCD), variable temperature, variable field MCD (VTVH MCD), and resonance Raman (rR) spectroscopic properties of the Fe-S clusters contained in Ni-deficient CODH. Essentially homogeneous sample preparations aided in the resolution of the reduced $[4Fe4S]^{1+}$ ($S = {}^1/_2$) B cluster and the reduced Ni-deficient C cluster (denoted C*, $S > {}^1/_2$) by MCD. The three Fe atoms derived from the [Ni3Fe4S] cubane component appear to dominate the reduced C* cluster MCD spectrum, while the presence of a fourth Fe center can be inferred from the ground state spin. The same underlying MCD features present in Ni-deficient CODH spectra are also observed for Ni-containing CODH, suggesting that both proteins contain the same C cluster Fe-S component. Overlooked in all spectroscopic studies to date, the D cluster was confirmed by rR to be a typical [4Fe4S] site with cysteinyl coordination. Together, MCD and rR data show that the D cluster remains in the oxidized $[4Fe4S]^{2+}$ ($S = 0$) state at potentials ≥ -530 mV (versus SHE), thus exhibiting an unusually low redox potential for a standard $[4Fe4S]^{2+/1+}$ electron-transfer site.

Carbon monoxide dehydrogenases (CODHs),[1] a class of Ni-containing enzymes that catalyze the reversible oxidation of CO to CO_2 (eq 1), occur in a variety of acetogenic,

$$CO + H_2O \rightarrow CO_2 + 2H^+ + 2e^- \qquad (1)$$

methanogenic, photosynthetic, and sulfate-reducing bacteria (*1*). While acetogenic and methanogenic bacterial CODHs contain an additional subunit that catalyzes the synthesis of acetyl-CoA (*1*−*3*), the CODH from the photosynthetic bacterium *Rhodospirillum rubrum* is only equipped to perform CO/CO_2 redox chemistry (*1*, *4*−*6*). Relying on CO as both carbon and energy sources under anaerobic conditions in the dark (*7*), *R. rubrum* utilizes CO-induced CODH in conjunction with a CO-induced hydrogenase to carry out an overall reaction, $CO + H_2O \rightarrow CO_2 + H_2$ ($\Delta G° = -20$kJ/mol) (*8*), equivalent to the industrial water−gas shift reaction (*1*).

Previously believed to be a 67 kDa monomer, *R. rubrum* CODH was recently crystallized as a 137 kDa homodimer and likely functions as such in vivo (*9*). Preliminary X-ray data at moderate resolution (3.3 Å) revealed two polynuclear metal clusters per monomer, termed B and C, and one additional cluster, termed D, at the monomer/monomer interface (*9*). While electron densities at the B and D sites were consistent with typical [4Fe4S] clusters, density in the region of the NiFeS-containing active site C cluster was ambiguous. The ill-defined region appeared consistent with the model developed by Münck and co-workers involving a Ni atom bridged to a [4Fe4S] cluster via a Cys residue (*10*, *11*). However, a high-resolution (1.6 Å) crystal structure of the CODH derived from *Carboxydothermus hydrogenoformans*, published by Dobbek et al. (*12*) while this paper was in review, revealed that the C cluster is actually a novel asymmetric [Ni4Fe5S] cluster, with all four Fe atoms bridged to the Ni ion by labile sulfur ligands (Figure 1).

Multiple polynuclear metal clusters give rise to particularly complex redox behavior in the case of CODH (*1*, *10*, *11*, *13*). The B cluster exists in two oxidation states, a diamagnetic $[4Fe4S]^{2+}$ state (B_{ox}) and a one-electron reduced $S = {}^1/_2$ $[4Fe4S]^{1+}$ state (B_{red}), consistent with its putative role as an electron-transfer center (*9*−*11*). The C cluster is stable in at least three oxidation states: an EPR-silent oxidized state (C_{ox}); a one-electron reduced $S = {}^1/_2$ state (C_{red1}) that exhibits a rhombic EPR spectrum with g values of 2.03, 1.88, and

[†] The work described here was supported by the University of Wisconsin and Petroleum Research Fund Grant ACS-PRF 35685-G3, administered by the American Chemical Society (T.C.B.), DOE Basic Energy Sciences Program Grant DE-FG02-87ER13691 (P.W.L.), and the NSF Graduate Research Fellowship Program (J.L.C.).

* Corresponding author. E-mail: brunold@chem.wisc.edu.

[‡] Department of Chemistry.

[§] Department of Biochemistry.

[1] Abbreviations: CODH, carbon monoxide dehydrogenase; Ni-CODH, Ni-containing CODH; Zn-CODH, Zn-substituted CODH; EPR, electron paramagnetic resonance; MCD, magnetic circular dichroism; VTVH MCD, variable temperature, variable field MCD; rR, resonance Raman; MOPS, 3-(*N*-morpholino)propanesulfonic acid; SDS−PAGE, sodium dodecyl sulfate−polyacrylamide gel electrophoresis; ICP-MS, inductively coupled plasma mass spectrometry; SHE, standard hydrogen electrode; PEG, poly(ethylene glycol); CCD, charge-coupled device; ZFS, zero-field splitting; HiPIP, high-potential iron protein; HCP, hybrid cluster protein.

10.1021/bi011586k CCC: $22.00
Published on Web 01/08/2002

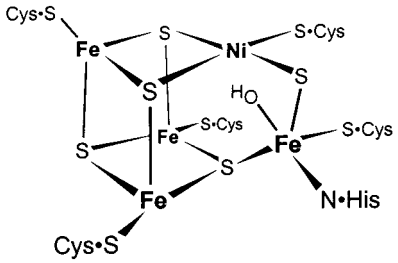

FIGURE 1: C cluster schematic adapted from ref *12*.

1.71; and another $S = {}^1/_2$ state (C_{red2}) with g values of 1.97, 1.87, and 1.75 (*10*, *11*). On the basis of EPR redox titrations, Heo et al. (*14*) proposed that one-electron reduction of the C_{red1} state in the absence of CO yields an additional $S = {}^1/_2$ state (C_{unc}) that exhibits g values of 2.04, 1.93, and 1.89 (identical to B_{red}). While X-ray data show the geometric arrangement of the five metal centers at the C cluster, the corresponding electronic structures of the various [Ni4Fe5S] oxidation states remain unclear (*12*, *15*). Interestingly, the presence of the third $[4Fe4S]_D$ cluster has been overlooked in all spectroscopic investigations to date. It is therefore possible that some of the spectral features originally assigned to the B and C clusters may actually arise from the D site.

One advantage of studying the CO oxidation system derived from *R. rubrum* relates to the ability to obtain Ni-deficient enzyme by growing the bacterium on Ni-depleted medium (*16*, *17*). With a full complement of Fe-S clusters, the Ni-deficient species cannot carry out CO/CO_2 redox chemistry but can be reactivated by incubation with aqueous Ni(II). In the absence of Ni, C cluster redox, EPR, and Mössbauer properties are significantly altered (*10*, *11*). The Ni-deficient C cluster (denoted C*) has been obtained in two states, an EPR-silent oxidized form (C^*_{ox}) and a one-electron reduced form (C^*_{red}) that exhibits signals in the $g = 4-6$ region of the EPR spectrum (*10*, *11*). On the basis of EPR and Mössbauer spectra, Münck and co-workers proposed that C^*_{ox} and C^*_{red} correspond to $S = 0$ $[4Fe4S]^{2+}$ and $S = {}^3/_2$ $[4Fe4S]^{1+}$ states, respectively (*10*). However, this hypothesis appears inconsistent with recent X-ray data of Ni-containing CODH (Ni-CODH) (*12*, *15*).

Our efforts to elucidate the molecular mechanism by which CODH catalyzes CO/CO_2 interconversion are currently directed toward obtaining detailed electronic descriptions of the [Ni4Fe5S] oxidatation states. As the complexities associated with this site have generated much confusion in recent years, our initial spectroscopic studies have focused on the Ni-deficient form of the enzyme. These investigations benefit greatly from improved enzyme purification protocols and essentially homogeneous sample preparations (*18*). Additionally, crystal structures published while this paper was undergoing the review process disclosed the geometry of the active site (*12*, *15*), permitting us to refine our discussion of C cluster electronics in light of an accurate Ni-CODH structural description. Here, we employ magnetic circular dichroism (MCD) and variable temperature, variable field MCD (VTVH MCD) as well as resonance Raman (rR) spectroscopies, techniques previously shown to be potent probes of other FeS-containing metalloenzymes (*19*, *20*), to study the nature of the Fe-S clusters in Ni-deficient CODH. Results presented in this paper indicate that the three Fe atoms derived from the [Ni3Fe4S] cubane dominate the MCD spectrum and further suggest how C* cluster Fe centers couple to give at least two distinct oxidation states. Preliminary Ni-CODH MCD spectra imply that the Fe-S component in the native C cluster shares the same basic electronic structure.

EXPERIMENTAL PROCEDURES

Cell Growth and Enzyme Purification. Strain UR-2 was cultured in a medium that was, depending upon the experiment, either completely lacking Ni or supplemented with 0.05 mM $NiCl_2$, according to established procedures (*4*, *21*). All buffers used during culture growth and purification steps were passed through a metal-chelating column (Bio-Rad Chelex-100 cation-exchange resin) to avoid incorporation of undesired metals into the active site. Ni-deficient and Ni-containing CODHs were purified according to previous methods (*18*) using 100 mM 3-(*N*-morpholino)propanesulfonic acid (MOPS) buffer, pH 7.5, and omitting the hydroxylapatite column step in the case of the Ni-deficient protein. Zn-substituted CODH (Zn-CODH) was obtained by incubation of Ni-deficient enzyme with 0.05 mM aqueous Zn(II) as described in the literature (*17*). Samples were determined from SDS−PAGE analysis to be greater than 95% pure.

Activity Assays and Metal Analyses. Activities are reported in units per milligram, where 1 unit = 1 μmol of oxidized CO/min. Enzyme metal content was determined by inductively coupled plasma mass spectrometry (ICP-MS) at the University of Georgia. The preparation of Ni-CODH had a specific activity of 12000 units/mg and contained 8.8 mol of Fe/monomer and 0.9 mol of Ni/monomer. The preparation of Ni-deficient CODH had a specific activity of <1 unit/mg and contained 8.5 mol of Fe/monomer and <0.001 mol of Ni/monomer. The preparation of Zn-CODH had a specific activity of <1 unit/mg and contained 8.8 mol of Fe/monomer, 0.9 mol of Zn/monomer, and <0.001 mol of Ni/monomer.

Sample Preparation. Unless otherwise indicated, all manipulations were performed in an anaerobic glovebox (Vacuum Atmospheres Model HE-493) under an N_2 atmosphere containing <1 ppm of O_2. Purified protein in 100 mM MOPS buffer, pH 7.5, containing 2 mM bicarbonate-free sodium dithionite was incubated with CO for 30 min to attain homogeneity. Upon application of the enzyme to a (diethylaminoethyl)cellulose column (Whatman DE-52), dithionite was removed by washing with 80 mM NaCl in 100 mM MOPS buffer, pH 7.5. The enzyme was eluted with buffer containing 200 mM NaCl and subsequently passed down a Sephadex G-25 column (Pharmacia Biotech) equilibrated with buffer to remove NaCl. All samples utilized in MCD experiments were then mixed with 60% (v/v) poly(ethylene glycol) (PEG 200) to ensure glass formation upon freezing. Nearly homogeneous oxidation states were prepared according to optimized procedures (*13*).

(a) Oxidized Ni-Deficient CODH. Ni-deficient CODH was titrated with thionin ($E_m{}^{\circ\prime} = +64$ mV versus SHE) until a faint blue color corresponding to oxidized dye persisted.

(b) Partially Reduced Ni-Deficient CODH. Ni-deficient CODH was transferred to an airtight metal-free quartz cuvette, placed into a UV−visible spectrophotometer, and titrated with concentrated bicarbonate-free dithionite until the absorption band at 420 nm decreased by approximately half ($E_m{}^{\circ\prime} \approx -300$ mV).

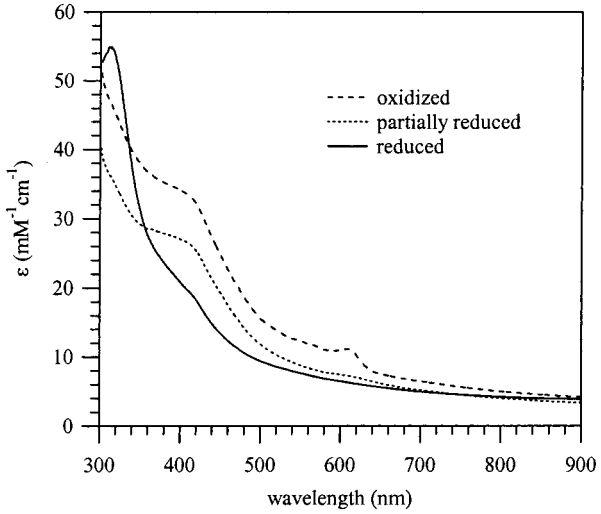

FIGURE 2: Absorption spectra of thionin-oxidized Ni-deficient CODH and dithionite-treated partially and fully reduced Ni-deficient CODH at 4 K in ~60% (v/v) PEG glasses. Absorption at 610 nm is attributed to the presence of excess thionin.

(c) Reduced Ni-Deficient, Zn-, and Ni-CODH. Purified protein samples were transferred to airtight metal-free quartz cuvettes, placed into a UV−visible spectrophotometer, and titrated with concentrated bicarbonate-free dithionite until the first appearance of dithionite absorption at 314 nm (final dithionite concentration of ~1 mM, $E_m{}^{\circ\prime} \approx -530$ mV).

MCD and rR Spectroscopy. MCD data were collected on a CD spectropolarimeter (Jasco J-715) with a sample compartment modified to accommodate a superconducting magnetocryostat (Oxford Instruments SM4-8T). A resonance Raman excitation profile for Ni-deficient CODH was recorded upon excitation with Ar^+ ion (Coherent I-305) and dye (Coherent 599-01) lasers with incident power in the 50−100 mW range. Scattering was collected at ~135° from the surface of frozen protein contained in an NMR tube immersed in a liquid N_2-filled EPR dewar. Scattered light was dispersed by a triple monochromator (Acton Research, equipped with 300, 1200, and 2400 grooves/mm gratings) and analyzed with a deep depletion, back-thinned CCD camera (Princeton Instruments Spec X: 100BR). Raman intensities were quantified relative to the 228 cm^{-1} scattering peak of ice.

RESULTS

The 4 K electronic absorption spectra of Ni-deficient CODH in ~60% (v/v) PEG glasses (Figure 2) were used to verify the redox states of the Fe-S clusters at several potentials. The strong absorption at 420 nm ($\epsilon_{420} \approx 34$ mM^{-1} cm^{-1}) of the thionin-oxidized sample arises from S → Fe^{3+} charge-transfer transitions (*19*) and is consistent with the presence of multiple $[4Fe4S]^{2+}$ clusters per CODH dimer. Both dithionite-treated samples contain reduced or partially reduced clusters, as evidenced by significant decreases in ϵ_{420}. Absorption spectra obtained at 300 K in the absence of PEG (not shown) are nearly identical to the 4 K data, indicating that the Fe-S cluster structures are preserved at cryogenic temperatures.

Variable field 4 K MCD spectra for Ni-deficient CODH at various potentials are shown in Figure 3. In contrast to the relatively featureless absorption spectra, MCD spectra

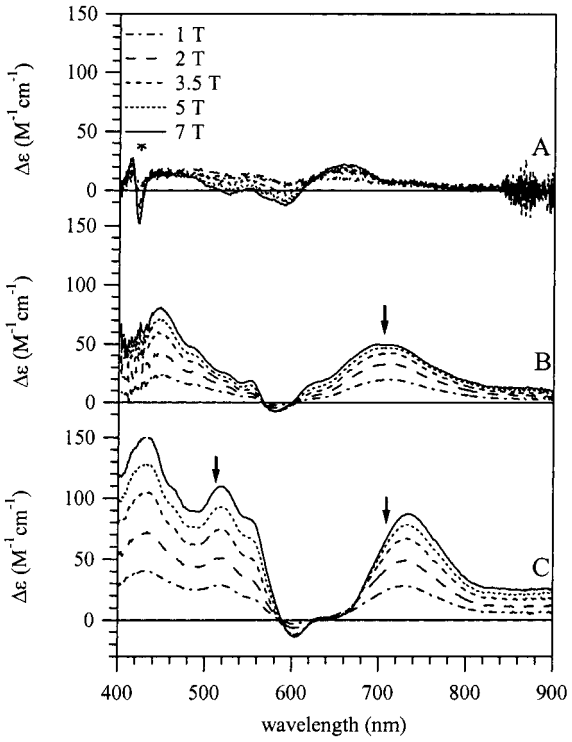

FIGURE 3: Variable-field 4 K MCD spectra of Ni-deficient CODH: (A) oxidized, (B) partially reduced, and (C) fully reduced. Arrows indicate wavelengths at which saturation data were obtained. The derivative-shaped feature (*) centered at 420 nm in the oxidized spectra indicates the presence of heme impurity (*31*).

vary significantly as a function of protein oxidation state. All MCD spectra exhibit several overlapping bands of predominantly positive intensity and differ substantially from those observed for typical [4Fe4S] clusters. MCD signals arising from paramagnetic species are strongly temperature dependent as a consequence of the Boltzmann population distribution among Zeeman-split sublevels of the electronic ground state (MCD *C*-term behavior) (*19*, *22*−*24*). Accordingly, significant increases in MCD intensities with decreasing temperature for all samples (Figure S1, Supporting Information) indicate that low-temperature spectra are dominated by paramagnetic chromophores.

Ground state spin information can be readily inferred from a VTVH MCD experiment, in which signal intensity at a specific wavelength is measured as a function of temperature and field. VTVH MCD data collected at 710 nm for the partially reduced enzyme and at both 510 and 710 nm for the fully reduced enzyme are presented in Figure 4 (solid lines). Theoretical magnetization curves for $S = {}^1/_2$, 1, ${}^3/_2$, 2, and ${}^5/_2$ species obtained using g values of 2.0 and omitting zero-field splittings (ZFS), so-called Brillouin curves, are also shown for comparison (dotted lines). Together, MCD spectra and VTVH MCD data obtained for partially reduced protein indicate that all spectral features exhibit the same field and temperature dependences and thus arise from a single paramagnetic species with $S > {}^1/_2$. Such VTVH behavior can be effectively modeled by an $S_{eff} = {}^5/_2$ Brillouin curve; however, it should be noted that Brillouin curves are not suitable for determining absolute ground state spins for systems with $S > {}^1/_2$ because ZFS effects inherent to low-symmetry protein sites are neglected (*23*−*25*). Conversely, the spectrum of the fully reduced protein exhibits field and

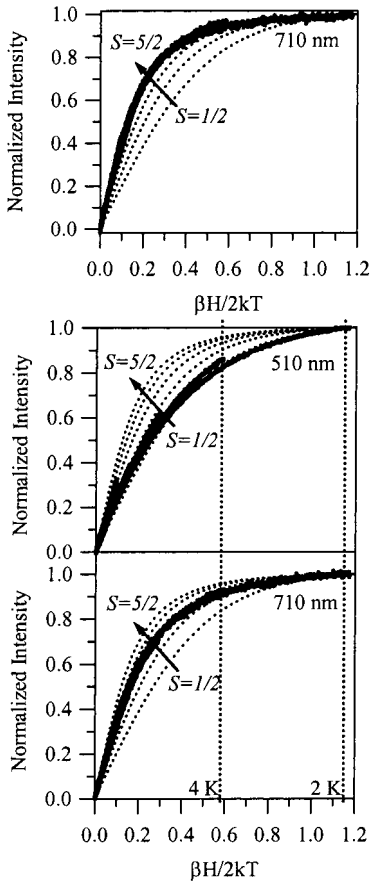

FIGURE 4: Ni-deficient CODH VTVH MCD data. Upper panel: Partially reduced Ni-deficient CODH data collected at 710 nm (cf. Figure 3). Lower panel: Fully reduced Ni-deficient CODH data collected at 510 nm (upper) and 710 nm (lower). Brillouin curves for $S = {}^1/_2$, 1, ${}^3/_2$, 2, and ${}^5/_2$ species obtained using g values of 2.0 and omitting zero-field splittings are also shown for comparison (dotted lines). Experimental conditions corresponding to 7 T and temperatures of 4 and 2 K are indicated by vertical dotted lines.

temperature dependences that vary as a function of wavelength, suggesting the presence of at least two paramagnets. VTVH MCD data indicate that the feature centered at 510 nm arises from an $S = {}^1/_2$ species, while the 710 nm feature requires contributions from a species with $S > {}^1/_2$. The VTVH behavior at the latter wavelength can be simulated using a 1:1 ratio of $S = {}^1/_2$ and $S = {}^5/_2$ Brillouin curves.

The spin states of the species contributing to the reduced Ni-deficient CODH spectrum are sufficiently different that spectral deconvolution is possible. As shown in Figure 4, the $S_{eff} = {}^5/_2$ component is essentially saturated at conditions corresponding to 7 T and 2 and 4 K, whereas the $S = {}^1/_2$ component is effectively saturated at 2 K but only ~80% saturated at 4 K. The $S = {}^1/_2$ component in the fully reduced protein could thus be isolated by subtracting the reduced protein spectrum obtained at 4 K from that obtained at 2 K. The difference spectrum, displaying features exclusively attributable to the $S = {}^1/_2$ species, was similar in general appearance to that observed for reduced [4Fe4S] clusters and was consequently rescaled to $\Delta\epsilon$ values typically observed for such species (*19*). Figure 5 presents the results from this spectral resolution: the upper two panels display the rescaled difference spectrum ($S = {}^1/_2$) and the partially reduced protein spectrum ($S_{eff} = {}^5/_2$), while the lower panel shows the corresponding sum spectrum (obtained by adding individual

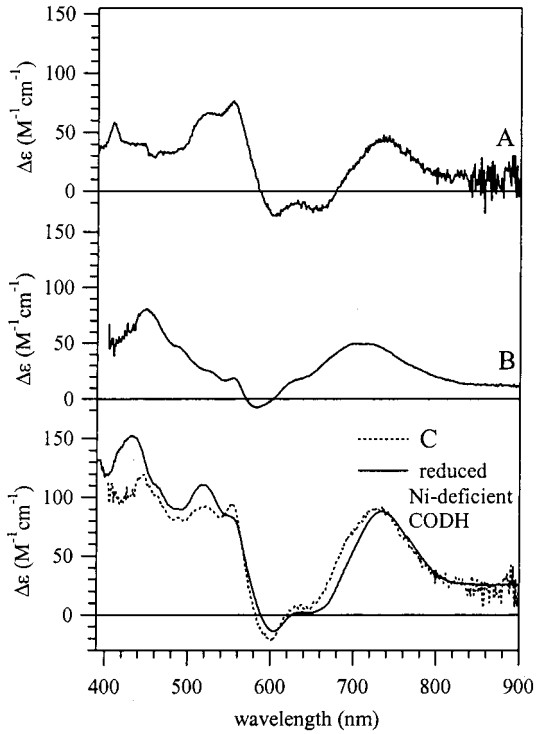

FIGURE 5: Resolution of individual paramagnetic clusters in Ni-deficient CODH. Spectrum A was obtained by subtracting the 7 T, 4 K MCD spectrum of reduced Ni-deficient CODH from that obtained at 7 T, 2 K in order to eliminate contributions from the $S_{eff} = {}^5/_2$ component. The difference spectrum was then rescaled to $\Delta\epsilon$ values typically observed for reduced [4Fe4S] clusters. Spectrum B corresponds to the spectrum of partially reduced Ni-deficient enzyme at 7 T and 4 K. Spectrum C, generated by adding spectra A and B, is plotted against the 7 T, 4 K spectrum obtained for reduced enzyme.

$S = {}^1/_2$ and $S_{eff} = {}^5/_2$ spectra) against the experimental spectrum of fully reduced Ni-deficient protein. This sum spectrum is indeed remarkably similar to that of reduced protein, lending credence to our analysis.

EPR studies on reduced Ni-deficient and Ni-containing CODHs have shown (*10*, *11*) that the $S = {}^1/_2$ signal is unperturbed upon removal of Ni from the active site, implying that this signal arises from B_{red}. In contrast, the $S = {}^3/_2$ signal observed for Ni-deficient enzyme is not present in Ni-CODH and has thus been attributed to C^*_{red}. On the basis of these results, it becomes relatively straightforward to assign the $S = {}^1/_2$ and the $S_{eff} = {}^5/_2$ MCD spectral features to B_{red} and C^*_{red}, respectively. This assignment is consistent with crystallographic (*9*) and Mössbauer (*10*) data, which also indicate that the B cluster is a typical [4Fe4S] cluster. The fact that the spectrum of the fully reduced enzyme corresponds to a ~1:1 ratio of the $S = {}^1/_2$ and $S_{eff} = {}^5/_2$ components suggests that contributions from the D cluster are minor, requiring that the $[4Fe4S]_D$ cluster remain in the diamagnetic 2+ oxidation state at potentials ≥ -530 mV. Such a low redox potential is rather atypical for [4Fe4S] clusters (*26*) and may explain why the D cluster has been overlooked in all spectroscopic studies to date.

Although the diamagnetism of $[4Fe4S]_D$ precludes characterization by MCD, the nature of this elusive cluster could be probed by rR spectroscopy on reduced Ni-deficient CODH (Figure 6). As shown by MCD, both B and C* Fe-S clusters are reduced and therefore expected to contribute minimally

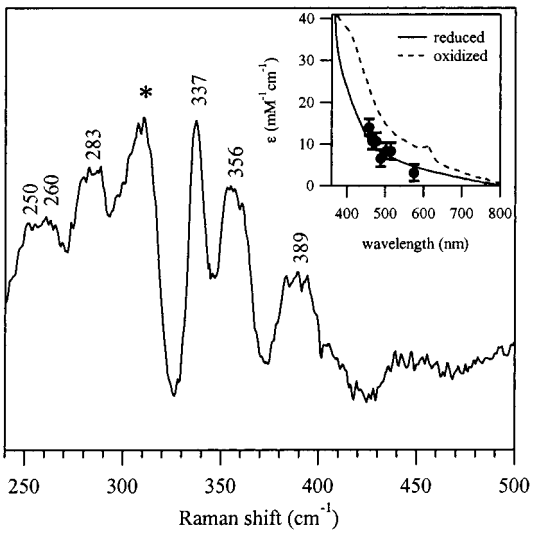

FIGURE 6: 77 K rR spectrum of ~1 mM reduced Ni-deficient CODH obtained using 457.9 nm laser excitation (100 mW laser power at sample, 2 h averaging time). The ice peak at 310 cm^{-1} is indicated (*). Inset: rR excitation profile (●) and corresponding low-temperature absorption spectrum for reduced protein, showing that all Fe-S stretching modes are resonance-enhanced by exciting near the S → Fe^{3+} charge-transfer absorption band. The absorption spectrum for oxidized protein is also shown for comparison.

Table 1: rR Features of Various Biological Clusters (*19*)[a]

cluster type	Fe-S stretching frequencies (cm^{-1})
1Fe	
D. gigas rubredoxin	126, **312**, 338, 359, 371
2Fe	
spinach ferredoxin	**284**, 328, 336, **395**, 425
3Fe	
D. gigas ferredoxin II	**260**, **345**, 365, 393
4Fe	
C. pasteurianum ferredoxin	**248**, 277, 298, **335**, **357**, 395
D. gigas ferredoxin I	**248**, 272, 289, **334**, **360**, 394

[a] Key features are highlighted in bold.

to rR spectra (*20*).[2] Thus, we attribute the features observed in the Fe-S stretching region (200−430 cm^{-1}) to the oxidized D cluster. Diagnostic of cluster structural variations, stretching frequencies observed for various Fe-S cluster types are listed in Table 1. Scattering peaks at 250, 260, 283, 337, 356, and 389 cm^{-1} indicate the presence of an oxidized [4Fe4S] cluster with cysteinyl coordination (*20*, *27*). All features in this region are resonance-enhanced by exciting near the S → Fe^{3+} charge-transfer absorption band, as shown in the corresponding excitation profile (Figure 6, inset). The most intense band at 337 cm^{-1} is assigned to symmetric stretching primarily involving the motion of μ_3-bridging sulfides (*28*−*30*). The frequency of this mode correlates with an average $Fe^{2.5+}$ oxidation state of a $[4Fe4S]^{2+}$ cluster, confirming that the monomer-bridging D cluster is a typical [4Fe4S] site (*28*−*30*).

As oxidizing dyes significantly reduce the stability of Ni-deficient CODH, spectroscopic data obtained on the thionin-treated species should be interpreted with caution. Figure 3A displays the highly unusual MCD spectra obtained on oxidized protein. Despite heme impurities that contribute to spectra at wavelengths below 600 nm (*31*),[3] several temperature-dependent bands can be resolved, all of which demonstrate saturation behavior characteristic of an $S > {}^1/_2$ species. As C^*_{ox} was previously shown to be EPR-silent, these results afford several possible scenarios: C^*_{ox} has an integer spin state with a large ZFS, or the paramagnetic species observed represents only a small fraction of Ni-deficient C cluster sites (i.e., physical mixture of $S = 0$ and $S > 0$ species or, alternatively, partial C cluster decomposition). While Mössbauer data reveal that the majority of the Fe atoms are in diamagnetic environments in thionin-oxidized protein, a significant fraction (ca. 0.25 spin/mol) of Fe atoms manifest features reminiscent of oxidized [3Fe4S] clusters (*10*). Because MCD spectra of oxidized Ni-deficient CODH are difficult to reproduce, spectral analysis remains a challenge. However, it is worthwhile to note that dithionite reduction of the thionin-oxidized sample resulted in a spectrum identical to that of the fully reduced protein. Such a result suggests that our oxidized sample contained the same clusters present in reduced samples, as opposed to primarily Fe-S cluster decomposition products.

DISCUSSION

Heterogeneous sample preparations have consistently posed a major challenge to past CODH spectroscopic studies (*1*). However, improved CODH purification procedures, as well as recognition that CO treatment of as-isolated enzyme significantly increases specific activity, recently culminated in the preparation of essentially homogeneous protein samples (*18*). Here we present the first successful CODH MCD and rR spectra, which permit new insight into the electronic nature of the C* cluster in Ni-deficient protein and the corresponding [Ni4Fe5S] site in Ni-CODH (vide infra).

Combined electronic absorption, MCD, and rR experiments on Ni-deficient CODH are consistent with the presence of two distinct [4Fe4S] clusters, corresponding to $[4Fe4S]_B$ and monomer-bridging $[4Fe4S]_D$ from the crystal structure (*9*, *12*, *15*). MCD spectra obtained on various oxidation states indicate that the redox-active $[4Fe4S]_B$ cluster cycles between 2+ ($S = 0$) and 1+ ($S = {}^1/_2$) states with a midpoint potential between −300 and −530 mV. These data support the hypothesis that the B cluster is involved in electron transfer. Conversely, $[4Fe4S]_D$ appears to remain in the diamagnetic 2+ oxidation state at potentials ≥−530 mV. The rR experiments presented here offer the first spectroscopic probe of the D cluster and confirm its assignment as a typical [4Fe4S] site despite its unusually low redox potential. While no direct evidence exists to show that $[4Fe4S]_D$ functions as an electron-transfer site, it is likely that this site can be reduced in vivo at catalytically relevant potentials and can consequently relay electrons between the protein and the physiological electron acceptor CooF (*32*). Instances in which Fe-S cluster redox potentials are substantially increased by altering local hydrogen bonding networks, for example, are well documented. In the case of [4Fe4S] cluster electron-

[2] Reduction of both biological and synthetic [4Fe4S] clusters is typically accompanied by a loss of discernible Raman features, as Fe-S complexes are inherently weak scatterers and thus require excitation within S → Fe^{3+} charge-transfer absorption bands to observe corresponding vibrational transitions.

[3] The sharp derivative centered at 420 nm is indicative of low-spin ($S = {}^1/_2$) Fe^{3+} heme (*31*).

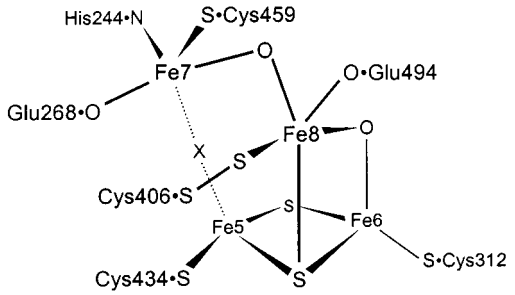

FIGURE 7: Schematic view of the putative active site in HCP protein adapted from ref *39*. X represents an unidentified, partially occupied site.

transfer proteins, namely, 4Fe ferredoxins and high-potential iron proteins (HiPIPs), the extent of hydrogen bonding to bridging sulfides greatly affects intracluster covalency and thus relative stabilities of oxidized and reduced [4Fe4S] clusters (*33*, *34*). Alternatively, an excessively low equilibrium redox potential does not necessarily dismiss the role of the D cluster in catalysis; e.g., the [NiFe] hydrogenase from *Chromatium vinosum* demonstrates remarkably efficient catalytic H_2 oxidation activity despite the high redox potential (~300 mV above catalytic potentials) of a $[3Fe4S]^{1+/0}$ electron-transfer cluster (*35*).

A particularly revealing aspect of these studies comes in resolution of the C cluster by MCD. Previous models involving a standard [4Fe4S] cubane at the CODH active site are readily discounted on the basis of Ni-deficient protein MCD spectra. The C^*_{red} spectrum, exhibiting saturation behavior characteristic of a species with $S > {}^1/_2$, is distinctly different in form from a typical $S = {}^3/_2$ $[4Fe4S]^{1+}$ spectrum (*19*, *27*). Rather, the general appearance and relative band intensities (Figure 3B) are strongly characteristic of reduced [3FeXS] clusters (*19*, *27*, *36*). In view of recent Ni-CODH crystal structures (*12*, *15*), dominant contributions to the Ni-deficient CODH MCD spectrum appear to originate from the three Fe atoms comprising the [Ni3Fe4S] cubane. These results indicate that the fourth Fe atom is likely reduced in the C^*_{red} state, and while spin coupling between the 3Fe component and this species may be significant, this metal center contributes minimally to spectral intensity.

While [3FeXS] clusters present a valuable comparison, it is also interesting to note the striking spectral similarities exhibited by C^*_{red} in Ni-deficient CODH and the putative active site (*37*) of reduced hybrid cluster protein (HCP, formerly known as "prismane" protein), an Fe-S protein of unknown function that shares significant structural and sequence similarity with *R. rubrum* CODH (*38*). Although HCP was originally believed to contain a [6Fe6S] cluster on the basis of spectroscopic data, X-ray studies revealed that the protein actually contains two 4Fe clusters some 12 Å apart (*37*, *39*). The proposed active site, a novel 4Fe structure with two μ_2-sulfido bridges, two μ_2-oxo bridges, and an unidentified partially occupied μ_2 bridge X, is depicted in Figure 7. Despite differences in Fe atom arrangement and metal cluster ligands, both HCP and CODH contain a 3Fe component bridged to a fourth Fe with partial His coordination (cf. Figures 1 and 7), suggesting possible evolutionary ties (*12*, *15*, *40*).

Although the HCP active site is formally a 4Fe cluster, spectroscopic studies by Thomson and co-workers (*38*) show

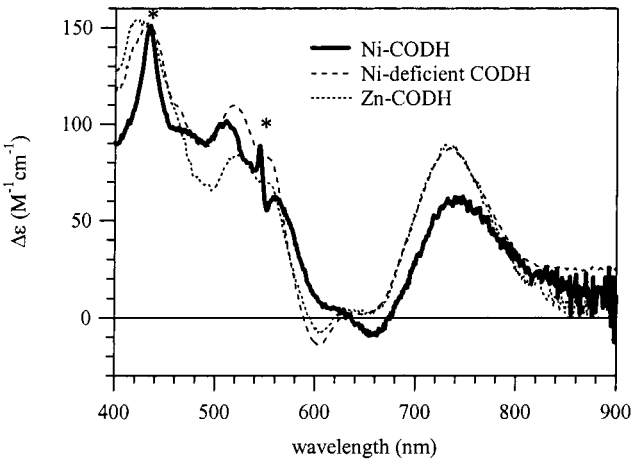

FIGURE 8: MCD spectra of Ni-deficient CODH, Zn-CODH, and Ni-CODH at 7 T and 4 K. Protein concentrations ranged from ~0.3 to 1 mM. Heme impurities present in the Ni-CODH sample are indicated (*) (*31*, *41*).

that the MCD spectrum of the fully reduced enzyme (the so-called "3+" state in which Fe7 and Fe8 are Fe^{2+}) resembles that of a 3Fe cluster. While similar in form to a [3FeXS] site, the spectrum appears to derive most of its intensity from the Fe5/Fe6 [2Fe2S] cluster subcomponet; i.e., one-electron oxidation of this mixed-valence Fe^{3+}/Fe^{2+} pair in 3+ HCP results in a strikingly different spectrum of greatly reduced intensity.[4] In contrast to the C* cluster of Ni-deficient CODH ($S > {}^1/_2$, likely $S = {}^3/_2$ based on previously reported EPR results), however, reduced 3+ HCP exhibits $S = {}^1/_2$ magnetization behavior (*38*). Thus, the relative arrangement of four Fe centers appears to appreciably affect intercluster exchange coupling: the oxo-bridged Fe in HCP couples with the 3Fe component to give an $S = {}^1/_2$ ground state, whereas the arrangement of the four Fe atoms in the reduced C* cluster results in an $S > {}^1/_2$ ground state.

Interestingly, one-electron oxidation of the C^*_{red} cluster leads to a substantial change in form and intensity of the MCD spectrum (Figure 3A). Although the corresponding spectrum differs qualitatively from that of the "4+" HCP active site (*38*), both the low MCD intensity and the nesting behavior of VTVH MCD data of C^*_{ox} are consistent with a similar mixture of $S = 0$ and $S = 4$ spin states as observed for HCP. Conversely, oxidized protein spectra differ considerably from those of standard $S = 2$ $[3FeXS]^0$ clusters (which would be obtained upon one-electron oxidation of a $[3FeXS]^{1-}$ C^*_{red} cluster), as these clusters typically exhibit intense MCD *C*-terms (*27*, *36*). Thus, while we have no direct spectroscopic evidence for the presence of four Fe atoms at the C* cluster, our data appear most consistent with a similar spin-coupling scheme as observed for HCP; i.e., a 3Fe subcomponent in reduced protein provides dominant spectral contributions, while a fourth Fe center influences the C* cluster ground state spin through exchange coupling.

Figure 8 compares MCD spectra of reduced Zn-CODH and Ni-CODH to that of reduced Ni-deficient enzyme. As Zn remains in the 2+ oxidation state throughout, it is

[4] While both Fe-S clusters are paramagnetic in the 3+ state and thus contribute to the MCD spectrum, VTVH MCD data by Thomson and co-workers (*38*) reveal that the dominant features arise from an $S = {}^1/_2$ species (the hybrid cluster), not the $S = {}^3/_2$ species (the $[4Fe4S]^{1+}$ cluster).

presumed to act as a Ni "place holder" that is electronically decoupled from the C cluster Fe-S component. Nearly identical Zn-substituted and Ni-deficient enzyme spectra suggest that the C cluster Fe-S structure is conserved in Ni-deficient protein; i.e., removal of Ni does not drastically distort the geometry of the Fe-S site.

The same underlying features present in Ni-deficient and Zn-substituted CODH spectra are also observed in the Ni-CODH spectrum (Figure 8), suggesting that all species contain the same basic Fe-S component (*31*, *41*).[5] There are, however, small but significant differences between the Ni-deficient and Zn-substituted CODH spectra and the Ni-CODH spectrum, most visibly near 600 nm where additional positive intensity is observed in the latter spectrum. These data suggest that the presence of Ni (but not Zn) perturbs the electronic structure of the C cluster, consistent with EPR and Mössbauer spectroscopic data (*10*, *11*, *14*).

Future research aimed at elucidating the [Ni4Fe5S] cluster electronics and corresponding reactivity of Ni-CODH will benefit considerably from the studies on the Ni-deficient protein presented herein. We anticipate that the pure B_{red} and C^*_{red} cluster spectra will permit us to resolve spectral subtleties associated with the Ni site as well as the interaction of the active site cluster with substrate (analogues).

ACKNOWLEDGMENT

We thank Drs. Jongyun Heo and Christopher R. Staples for insightful discussion and the preparation of protein samples (J.H.).

SUPPORTING INFORMATION AVAILABLE

One figure showing variable temperature 7 T MCD spectra of Ni-deficient CODH samples. This material is available free of charge via the Internet at http://pubs.acs.org.

REFERENCES

1. Ragsdale, S. W., and Kumar, M. (1996) *Chem. Rev. 96*, 2515−2539.
2. Drake, H. L. (1994) *Acetogenesis*, Chapman & Hall, New York.
3. Ferry, J. G. (1993) *Methanogenesis*, Chapman & Hall, New York.
4. Bonam, D., and Ludden, P. W. (1987) *J. Biol. Chem. 262*, 2980−2987.
5. Stephens, P. J., McKenna, M. C., Ensign, S. A., Bonam, D., and Ludden, P. W. (1989) *J. Biol. Chem. 264*, 16347−16350.
6. Tan, G. O., Ensign, S. A., Ciurli, S., Scott, M. J., Hedman, B., Holm, R. H., Ludden, P. W., Korsun, Z. R., Stephens, P. J., and Hodgson, K. O. (1992) *Proc. Natl. Acad. Sci. U.S.A. 89*, 4427−4431.
7. Kerby, R. L., Ludden, P. W., and Roberts, G. P. (1995) *J. Bacteriol. 177*, 2241−2244.
8. Fox, J. D., Kerby, R. L., Roberts, G. P., and Ludden, P. W. (1996) *J. Bacteriol. 178*, 1515−1524.
9. Drennan, C. L., Spangler, N. J., Ludden, P. W., and Rees, D. C. (1999) *J. Inorg. Biochem. 74*, 118−118.
10. Hu, Z. G., Spangler, N. J., Anderson, M. E., Xia, J. Q., Ludden, P. W., Lindahl, P. A., and Münck, E. (1996) *J. Am. Chem. Soc. 118*, 830−845.
11. Spangler, N. J., Lindahl, P. A., Bandarian, V., and Ludden, P. W. (1996) *J. Biol. Chem. 271*, 7973−7977.
12. Dobbek, H., Svetlitchnyi, V., Gremer, L., Huber, R., and Meyer, O. (2001) *Science 293*, 1281−1285.
13. Heo, J., Staples, C. R., and Ludden, P. W. (2001) *Biochemistry 40*, 7604−7611.
14. Heo, J., Staples, C. R., Telser, J., and Ludden, P. W. (1999) *J. Am. Chem. Soc. 121*, 11045−11057.
15. Drennan, C. L., Heo, J., Sintchak, M. D., Schreiter, E., and Ludden, P. W. (2001) *Proc. Natl. Acad. Sci. U.S.A. 98*, 11973−11978.
16. Bonam, D., McKenna, M. C., Stephens, P. J., and Ludden, P. W. (1988) *Proc. Natl. Acad. Sci. U.S.A. 85*, 31−35.
17. Ensign, S. A., Campbell, M. J., and Ludden, P. W. (1990) *Biochemistry 29*, 2162−2168.
18. Heo, J., Staples, C. R., Halbleib, C. M., and Ludden, P. W. (2000) *Biochemistry 39*, 7956−7963.
19. Johnson, M. K., Robinson, A. E., and Thomson, A. J. (1982) in *Iron−Sulfur Proteins* (Spiro, T. G., Ed.) pp 367−406, Wiley-Interscience, New York.
20. Spiro, T. G., Hare, J., Yachandra, V., Gewirth, A., Johnson, M. K., and Remsen, E. (1982) in *Iron−Sulfur Proteins* (Spiro, T. G., Ed.) pp 407−423, Wiley, New York.
21. Ensign, S. A., Bonam, D., and Ludden, P. W. (1989) *Biochemistry 28*, 4968−4973.
22. Piepho, S. B., and Schatz, P. N. (1983) *Group Theory in Spectroscopy with Applications to Magnetic Circular Dichroism*, Wiley, New York.
23. Neese, F., and Solomon, E. I. (1999) *Inorg. Chem. 38*, 1847−1865.
24. Oganesyan, V. S., George, S. J., Cheesman, M. R., and Thomson, A. J. (1999) *J. Chem. Phys. 110*, 762−777.
25. Solomon, E. I., Paverl, E. G., Loeb, K. F., and Campochiaro, C. (1995) *Coord. Chem. Rev. 144*, 369−460.
26. Holm, R. H., Kennepohl, P., and Solomon, E. I. (1996) *Chem. Rev. 96*, 2239−2314.
27. Conover, R. C., Kowal, A. T., Fu, W., Park, J.-B., Aono, S., Adams, M. W. W., and Johnson, M. K. (1990) *J. Biol. Chem. 265*, 8533−8541.
28. Johnson, M. K., Czernuszewicz, R. S., Spiro, T. G., Fee, J. A., and Sweeney, W. V. (1983) *J. Am. Chem. Soc. 105*, 6671−6678.
29. Czernuszewicz, R. S., Macor, K. A., Johnson, M. K., Gewirth, A., and Spiro, T. G. (1987) *J. Am. Chem. Soc. 109*, 7178−7187.
30. Backes, G., Mino, Y., Loehr, T. M., Meyer, T. E., Cusanovich, M. A., Sweeney, W. V., Adman, E. T., and Sanders-Loehr, J. (1991) *J. Am. Chem. Soc. 113*, 2055−2064.
31. Dawson, J. H., and Dooley, D. M. (1989) in *Physical Bioinorganic Chemistry Series* (Lever, A. B. P., and Gray, H. B., Eds.) pp 1−135, VCH Publishers, Inc., New York.
32. Ensign, S. A., and Ludden, P. W. (1991) *J. Biol. Chem. 266*, 18395−18403.
33. Glaser, T., Rose, K., Shadle, S. E., Hedman, B., Hodgson, K. O., and Solomon, E. I. (2001) *J. Am. Chem. Soc. 123*, 442−454.
34. Glaser, T., Bertini, I., Moura, J. J. G., Hedman, B., Hodgson, K. O., and Solomon, E. I. (2001) *J. Am. Chem. Soc. 123*, 4859−4860.
35. Pershad, H. R., Duff, J. L. C., Heering, H. A., Duin, E. C., Albracht, S. P. J., and Armstrong, F. A. (1999) *Biochemistry 38*, 8992−8999.
36. Johnson, M. K., Bennett, D. E., Fee, J. A., and Sweeney, W. V. (1987) *Biochim. Biophys. Acta 911*, 81−94.
37. Cooper, S. J., Garner, C. D., Hagen, W. R., Lindley, P. F., and Bailey, S. (2000) *Biochemistry 39*, 15044−15054.
38. Marritt, S. J., Farrar, J. A., Breton, J. L. J., Hagen, W. R., and Thomson, A. J. (1995) *Eur. J. Biochem. 232*, 501−505.

[5] The sharp temperature-independent derivative centered at 548 nm is characteristic of low-spin ($S = 0$) Fe^{2+} heme, and the positive band at 435 nm is typical of that observed for a trace of high-spin ($S = 2$) Fe^{2+} heme (*31*, *41*).

39. Arendsen, A. F., Hadden, J., Card, G., McAlpine, A. S., Bailey, S., Zaitsev, V., Duke, E. H. M., Lindley, P. F., Kröckel, M., Trautwein, A. X., Feiters, M. C., Charnock, J. M., Garner, C. D., Marritt, S. J., Thomson, A. J., Kooter, I. M., Johnson, M. K., van den Berg, W. A. M., van Dongen, W. M. A. M., and Hagen, W. R. (1998) *J. Biol. Inorg. Chem. 3*, 81−95.

40. van den Berg, W. A. M., Hagen, W. R., and van Dongen, W. A. M. (2000) *Eur. J. Biochem. 267*, 666−676.

41. Thomson, A. J., and Johnson, M. K. (1980) *Biochem. J. 191*, 411−420.

BI011586K